

# Three-Level Biomimetic Rice-Leaf Surfaces with Controllable Anisotropic Sliding

Dong Wu, Jian-Nan Wang, Si-Zhu Wu, Qi-Dai Chen,\* Shuai Zhao, Hao Zhang, Hong-Bo Sun,\* and Lei Jiang

Rice leaves with anisotropic sliding properties have the ability to directionally control the movement of water microdroplets. However, the realization of artificial anisotropic sliding biosurfaces has remained challenging. It is found, by a systematic investigation, that the height of 200- $\mu\text{m}$ -width groove arrays on rice leaves reaches up to 45  $\mu\text{m}$ , far greater than the smaller microgrooves that are widely adopted for the study of anisotropic wetting. A new model based on three-level microstructures (macro/micro/nano) is developed to interpret the anisotropic sliding behavior. Moreover, artificial rice leaves with different macrogrooves are demonstrated by combining micro/nanostructures and macrogrooves, which are prepared by photolithography, PDMS imprinting, and micro/nanostructure coating. Sliding-angle measurement further prove that the third-level macrogroove arrays are the determining factor for anisotropic sliding. Finally, a new testing method, curvature-assisted droplet oscillation (CADO), is developed to quantitatively reveal the anisotropic dynamic behavior of biomimetic rice-leaf-like surfaces.

crucial for water droplets to move along the leaf veins and finally to the root, helping the plants to survive. It is recognized that the quasi-1D arrangement of micropapilla ( $\approx 5 \mu\text{m}$ ) covered with nanoscale surface features, namely a micro- and nano-, two-level hierarchical structure, leads to the observed anisotropic wetting. Inspired by this natural phenomenon, artificial anisotropic surfaces that mimic the quasi-1D microstructures of a rice leaf have attracted great attention for their important potential applications in fluidic control, water-directional transportation, and so on.<sup>[5,6]</sup> A variety of technologies<sup>[7–13]</sup> such as photolithography,<sup>[7,8]</sup> surface wrinkling,<sup>[9]</sup> electrospinning,<sup>[10]</sup> and interference lithography<sup>[11,12]</sup> has been used to reproduce the biomimetic surfaces. Specifically, the smaller (width 0.3–20  $\mu\text{m}$  and height 0.05–5  $\mu\text{m}$ ) groove arrays<sup>[7,9–12,13a–d]</sup>

## 1. Introduction

Anisotropic microstructured surfaces allow water striders to walk on water,<sup>[1]</sup> butterflies to shed water from their body's center-axis,<sup>[2]</sup> and rice leaves to guide water microdroplets.<sup>[3]</sup> Although the microstructures and functions of water-strider legs and butterfly wings have been mimicked recently,<sup>[4]</sup> the anisotropy of the rice leaf has not been demonstrated. Rice leaves exhibit the ability to directionally control the motion of water microdroplets, namely anisotropic wetting. The droplet can freely roll, due to the Cassie surface state<sup>[3]</sup>, and the sliding angles along the parallel and perpendicular directions of a rice leaf are different, at approximately 3° and 9°, respectively. This anisotropic-sliding ability is

have been widely prepared to mimic the quasi-1D microstructures of the rice leaf and have become the most common microstructures used for investigating anisotropic wetting properties. For example, Morita et al.<sup>[7]</sup> reported macroscopic anisotropic wetting on line-patterned surfaces prepared by vacuum-UV lithography, Zhao et al.<sup>[11a]</sup> prepared anisotropic sub-micrometric periodic groove arrays on azobenzene-containing multiarm star-polymer films, and Xia et al.<sup>[12a]</sup> realized strongly anisotropic wetting on nanopatterned surfaces by multibeam-laser interference. Anisotropic contact angles from 5° to 79° have been successfully produced by designing different groove arrays, leading to great progress in the reproduction of the rice-leaf structure. Nevertheless, until now, the excellent anisotropic-sliding ability ( $\approx 3^\circ/9^\circ$ ) of the rice leaf, the most important expected function, has not been realized. Moreover, precise control of the anisotropic-sliding behavior remains challenging, possibly the direct result of insufficient understanding of the physical mechanism of anisotropic sliding. An apparent example is that artificial surfaces reported so far have focused on single-level groove arrays with of smaller size, which suffer from low contact angle (CA) so that the water droplet in Wenzel's state cannot freely roll. In addition, the technical challenge of characterizing anisotropic-dynamic behavior hinders deep insight into the underlying physics of anisotropic sliding. In detail, static CAs along the parallel and perpendicular directions of one surface are generally used to depict anisotropy because the water droplet is in the pinned state with a small contact angle.<sup>[7–12]</sup> However, for anisotropic surfaces with excellent superhydrophobicity (CA larger than 150°), it is insufficient to evaluate the anisotropic wetting by using CAs. In this case, the sliding angle

Dr. D. Wu, J. N. Wang, S. Z. Wu, Dr. Q. D. Chen, S. Zhao, H. Zhang,  
Prof. H.-B. Sun

State Key Laboratory on Integrated Optoelectronics  
College of Electronic Science and Engineering  
Jilin University  
2699 Qianjin Street, Changchun, 130012, China  
E-mail: chenqd@jlu.edu.cn; hbsun@jlu.edu.cn

Prof. L. Jiang  
Center of Molecular Sciences, Institute of Chemistry  
Chinese Academy of Sciences, Beijing, 10190, China

Prof. H.-B. Sun  
College of Physics  
Jilin University  
119 Jiefang Road, Changchun, 130023, China

DOI: 10.1002/adfm.201002733

(SA) becomes the most important parameter in characterizing the water hysteresis,<sup>[3,14–21]</sup> which is determined by the surface frictional coefficient. However, the frictional force of the water droplet on the rice leaf is so small that it is very difficult to measure.

Herein, after a careful study of the real rice leaf, we found that the height of the 200- $\mu\text{m}$ -width groove arrays<sup>[22]</sup> reached up to 45  $\mu\text{m}$ , far greater than that of the smaller microgrooves<sup>[7,9–12,13a–d]</sup> that are widely used to produce anisotropic wetting. We further reproduced a three-level hierarchical surface by combining photolithography, PDMS imprinting, and micro/nanostructure coating, and developed a new method, which we named curvature-assisted droplet oscillation (CADO), to quantitatively characterize the weak frictional interaction between the liquid droplet and the structured surface. These results show that each of the three-level hierarchical structures plays an indispensable role in the anisotropic-sliding functionality; the micro/nanostructures enhance the contact angle to facilitate the free motion of droplets and the macrogrooves direct their anisotropic sliding.

## 2. Results and Discussion

### 2.1. Third-Level Structure on the Rice Leaf: Macrogroove Arrays

Shown in Figure 1a is the top view and magnified scanning-electron microscope (SEM) image of a rice leaf. Similar to that of other plants and insects, the surface of the rice leaf consists of dual-size structures; micrometer-scale papilla and nanostructures. However, these papilla seem to arrange in an orderly fashion along the longitudinal direction (direction of arrow

denoted by  $\parallel$ ), while they are irregularly arranged in the lateral direction (direction of arrow denoted by  $\perp$ ). The CA measurement shows that the water sliding angle is also different in both directions ( $SA_{\perp} = 3^{\circ}$ ,  $SA_{\parallel} = 9^{\circ}$ ; the water droplet is about 4  $\mu\text{L}$ ), as shown in Figure 1b. Thus, the anisotropy of the rice leaf has been widely attributed to the directional arrangement of micropapilla. However, from the 60°-tilted SEM image (Figure 1c), there is a special kind of microstructure; sub-millimeter-scale groove arrays. The width and depth of these arrays reach up to 200 and 45  $\mu\text{m}$  (Figure 1d), respectively. The grooves extend along the longitudinal direction, which is the predominant direction in which water rolls. Generally, the macrogroove arrays may hinder the movement of the water droplet and exhibit anisotropic wetting. So the sub-millimeter-scale grooves may guide the rolling of the water droplet. Based on this analysis, we put forward a new model (Figure 1e) to explain the anisotropic sliding property of the rice leaf. There are three-level geometrical structures on the surface of the rice leaf. The micro- and nano- hierarchical structures of the rice leaf are crucial to superhydrophobicity (Cassie's state), while the third-level macrogroove arrays provide an energy barrier to travel in orthogonal directions and contributes to the anisotropic sliding phenomenon.

### 2.2. Preparation of Artificial Biomimetic Rice Leaves with Different Height/Width Grooves

To verify our speculations, artificial biomimetic rice-leaf surfaces with sub-millimeter-scale grooves and micro/nanostructures were designed and prepared. Figure 2a shows the schematic illustration of the fabrication process of an artificial rice leaf (ARL). The fabrication generally consisted of three steps: photolithography, polydimethylsiloxane (PDMS) transfer, and micro/nanostructure coating. First, macrogroove arrays were prepared using UV photolithography. Then, the arrays were transferred by PDMS imprint lithography. After coating the arrays with micro/nanostructures (nanoporous polydivinylbenzene with excellent superhydrophobicity),<sup>[23]</sup> an ARL was formed. Furthermore, to systematically investigate the role of the macrogrooves, we prepared groove arrays with different depths (10, 20, 40, and 60  $\mu\text{m}$ ) and widths (20, 50, 100, 150, and 200  $\mu\text{m}$ ). Shown in Figure 2b–2d are top-view SEM images of ARLs with macrogrooves of different widths, which could be controlled by using a photomask. The grooved surface retained its morphology after being coated with the micro/nanostructures. As seen from the high-magnification SEM images (Figure 2e), the macrogroove arrays were covered with homogeneous micro/nanostructures. The ARL exhibited a high static contact angle ( $>160^{\circ}$ ) due to the excellent superhydrophobicity of the micro/nanostructures. The tilted-view SEM images (Figure 2f and 2g)

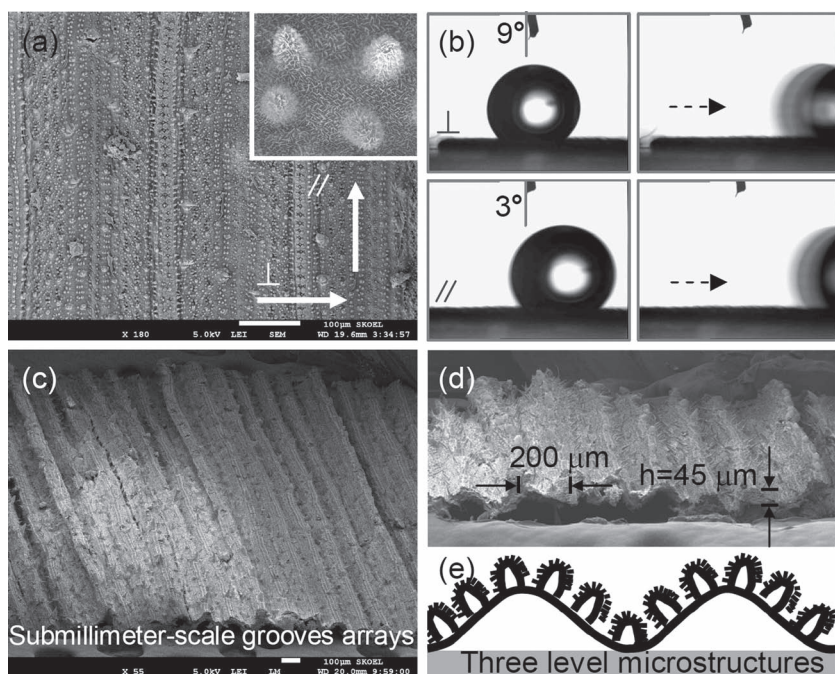


**Figure 1.** The anisotropic wetting of a rice leaf and the sub-millimeter-scale groove arrays. a) Top-view SEM image of the rice leaf. The inset is the magnified image of dual-size structures; micrometer-scale papilla and nanostructures. b) The anisotropic sliding property of the rice leaf. c) 60°-tilted-view SEM image of the rice leaf. d) Cross-sectional SEM image of the macrogrooves; width=200  $\mu\text{m}$  and height=45  $\mu\text{m}$ . e) Proposed three-level model of the rice leaf.

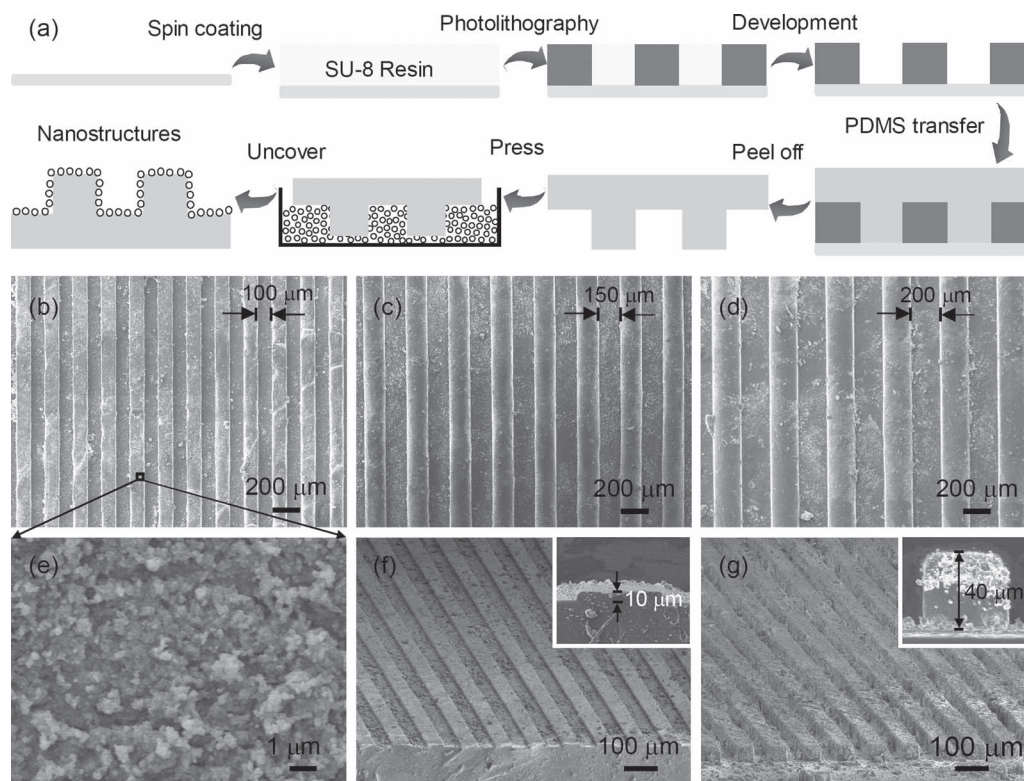


**Figure 2.** a) Schematic illustration of the fabrication process of ARLs, mainly consisting of three steps: photolithography, polydimethylsiloxane (PDMS) transfer, and micro/nanostructure coating. b-d) Top-view SEM images of ARLs with grooves of different widths. e) Magnified SEM image of the ARL. f) and g) ARLs with grooves of different heights. The insets are the 90°-tilted SEM images.

show the ARLs with grooves of different heights. The heights of the grooves were 10 and 40  $\mu\text{m}$ , controlled by the thickness of the resins, as seen from the cross-section SEM image (insets of Figure 2f and 2g).

### 2.3. SA Measurement and Physical Mechanism of Anisotropic Sliding

To investigate the directional control of the water-sliding ability, we measured the perpendicular and parallel sliding angles of the ARLs. The sample with 200- $\mu\text{m}$  width and 40- $\mu\text{m}$  height is similar to a natural rice leaf. Figures S1a and 1b in the Supporting Information show the optical microscopic images of water-droplet motion along the perpendicular and parallel directions. The measured SAs were 8° and 3°, respectively. The anisotropy was 5°, which is comparable to that of a natural rice leaf (6°), so this biomimetic surface has successfully mimicked the anisotropic sliding ability of the rice leaf. Furthermore, to explore the underlying mechanism of anisotropic sliding behavior, we systematically investigated the relationship between the macrogroove width and the anisotropy at different heights from 10–60  $\mu\text{m}$ , as shown in Figure 3a–3d. The measurement shows that the parallel SA along the direction of macrogrooves is very small, about 3° for all ARLs. However, the perpendicular SA depends on the parameters of grooves; height and width. From the comparison and analysis, we can

deduce two main rules. First, there are no obvious sliding anisotropy for the small-width groove. For example, when the groove width is less than 50  $\mu\text{m}$ , the anisotropy is very small (<2°) even if the groove height is >40  $\mu\text{m}$ . The reason for this disparity may be that the water droplet cannot reach the bottom of the smaller grooves, so that the effective height is much lower than the actual height, as shown in the schematic image 1 of Figure 3a–3d. This disparity results in the macro-groove arrays being unable to effectively hinder the movement of a water droplet in the perpendicular direction. Second, when the height of the grooves is too small (<10  $\mu\text{m}$ ), the surface also cannot exhibit anisotropic sliding behavior, as shown in Figure 3a. For all 10- $\mu\text{m}$ -height samples with different periods, the sliding anisotropy is less than 1°. This result is because this height is too small to effectively provide an energy barrier to affect the movement of water droplets. Therefore, both large height and width are crucial to the anisotropy sliding property. As the height becomes large (image 2 of Figure 3a–c), the anisotropy significantly increases, if the period is suitable. However, the anisotropy does not increase when the height reaches a certain value. For example, anisotropy reached a maximal value (5°) when the height was 40  $\mu\text{m}$ , because the water droplet could not reach the bottom of the 200- $\mu\text{m}$ -period grooves when the height was too large (60- $\mu\text{m}$  height, image 2 of Figure 3d). In this case, the sliding anisotropy could be further enhanced by increasing the groove width. From the above experimental results and comparative analysis, we believe that

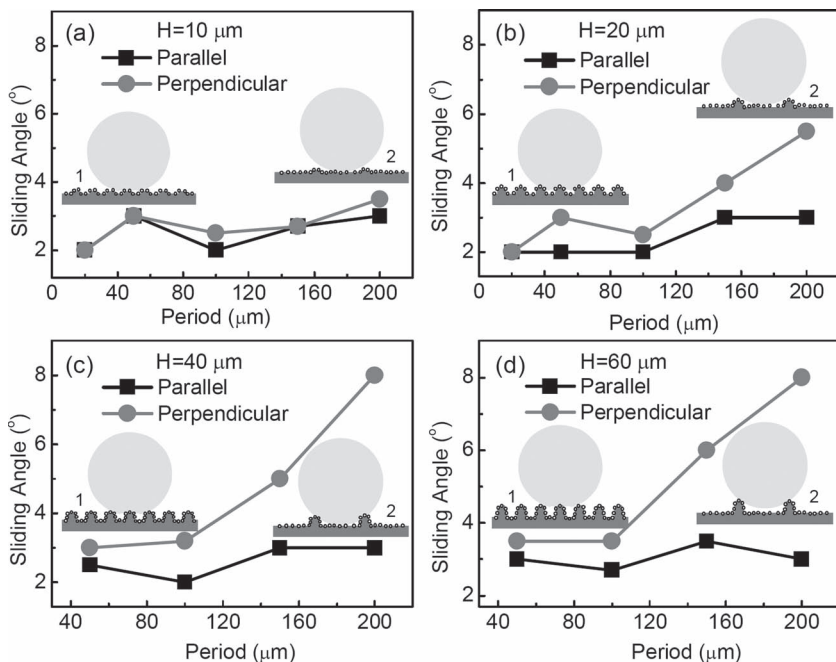


**Figure 3.** Sliding-angle measurement of different ARLs and the corresponding physical model. a–d) The relationship between groove width and anisotropy with different groove heights, from 10–60  $\mu\text{m}$ . The insets are the physical model of the water droplet on ARLs with different groove arrays.

the macrogroove arrays are the determining factor in sliding anisotropy. The common smaller microgrooves<sup>[7,9–12,13a–d]</sup> did not exhibit anisotropic sliding, even when they were combined

with nanostructures. Generally, the larger the period and height of the groove were, the more evident the directional dewetting was. According to this rule, the sliding anisotropy could be precisely controlled by designing the period and height of macrogroove arrays. In addition, the volume of the water droplet has an important impact on the anisotropy of an ARL. Generally, the larger the water droplet, the smaller the sliding angle.<sup>[13e]</sup> As shown in the Supporting Information Figure S2, the sliding anisotropy of the 200- $\mu\text{m}$ -period and 40- $\mu\text{m}$ -height ARL dramatically decreased when the volume increased. We found that there was no obvious sliding anisotropy when the volume of the water droplet was large than 16  $\mu\text{L}$ .

#### 2.4. Dynamic Anisotropic Sliding Evaluated by Curvature-Assisted Droplet Oscillation

The sliding angle characterizes the static water hysteresis. Here an original test (Figure 4), curvature-assisted water oscillation was implemented to quantitatively evaluate the dynamic sliding anisotropy of an ARL. First, the flexible PDMS surface was

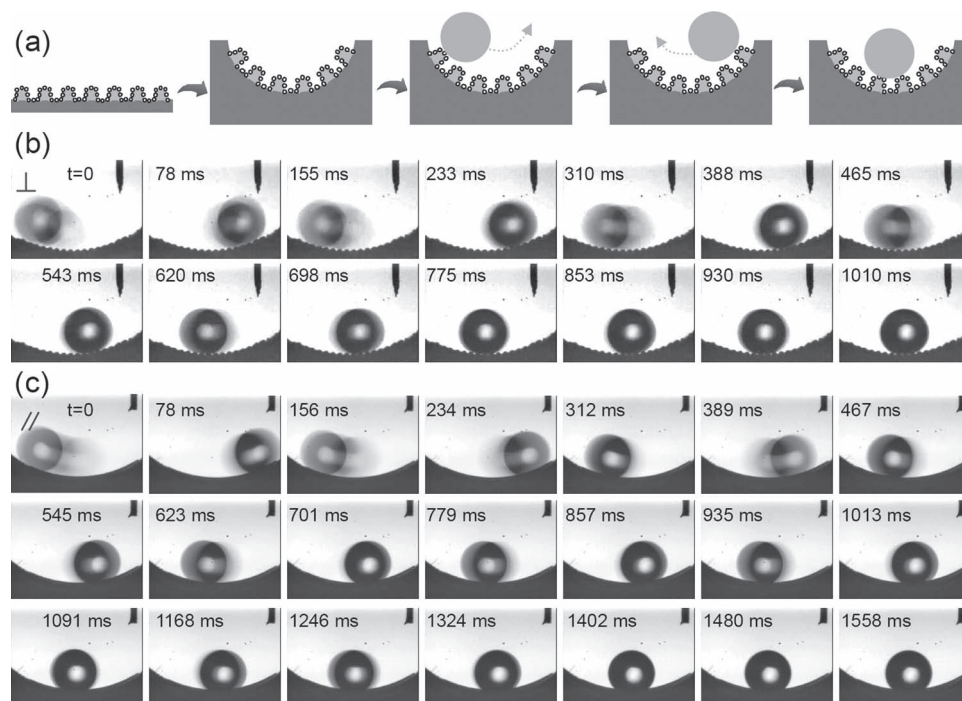


**Figure 4.** a) Illustration of the curvature-assisted droplet oscillation method, which evaluates the dynamic sliding anisotropy of one surface. b) and c) Dynamic oscillating behavior along the perpendicular and parallel directions. The oscillating time of the water droplet along the parallel direction is longer than that along the perpendicular direction. The oscillating difference could reflect the sliding anisotropy of both directions.

through the interaction of friction and gravity when it was put on the surface. Finally, it stopped because of the resistance force. Thus a simple oscillator formed. A water droplet was squeezed out from an appropriate initial height which could be adjusted by the position of the injector. Because the perpendicular resistance of the ARL was much greater than the parallel resistance, due to the energy barrier caused by macrogroove arrays, the dynamic oscillating behavior along both directions was different, which could reflect the anisotropy of the two directions, as shown in Figure 4b and 4c. From the above SA measurements, we know that the sample with larger grooves (both period and height) exhibits greater anisotropy. Hence, samples with 200- $\mu\text{m}$  width and 60- $\mu\text{m}$  height grooves were chosen for the dynamic test (Supporting Information videos 1 and 2). As shown in Figure 4, there was an obvious air gap under the droplet, which indicated that the sample was in the Cassie state. The water could overcome the weak drag force and move back and forth many times with gravitational potential. As seen from Figure 4b and 4c, in the parallel direction, the water droplet oscillated two rounds more than it did

in the perpendicular direction. This result demonstrates that the perpendicular resistance was much higher than the parallel resistance, just as expected.

## 2.5. Quantitative Analysis and Simulation by an Oscillating Model

Through fine analysis of the captured images, the relationship between the time and the angle [Supporting Information Table S1 and S2] was obtained, as shown by black squares in Figure 5a and 5b. We adopted an equivalent simple pendulum model [Supporting Information Figure S3] to simulate the experimental result. According to the kinematical equation of the simple pendulum<sup>[24]</sup> [Supporting Information and Equation (1)], the weak damping nonlinear resonance equation was simplified, by considering the existence of friction and the absence of a driving force.

$$\frac{d^2\theta}{dt^2} + \frac{g}{l} \sin\theta + q \frac{d\theta}{dt} = 0 \quad (1)$$

By introducing the parameter oscillation frequency  $\omega = \frac{d\theta}{dt}$ , we got  $\frac{d\omega}{dt} = -\frac{g}{l} \sin\theta - q\omega$ , where  $\theta$  is the angular displacement,  $q$  is the damping coefficient,  $g$  is the acceleration of gravity, and  $l$  is the pendulum length. Then, we fitted the theoretical curves with the experimental results, as shown in Figure 5a and 5b. According to the simulation, the damping coefficients in the two directions were obtained as  $q_{\parallel} = 2.95$  and  $q_{\perp} = 5.11$ . The value of  $q_{\perp}$  was 73% higher than  $q_{\parallel}$ , which quantitatively indicates that the water droplet has to overcome a much higher friction force when it rolls in the perpendicular direction. This result further demonstrates that the macrogroove arrays play a determining role in the anisotropic sliding behavior of the rice leaf.

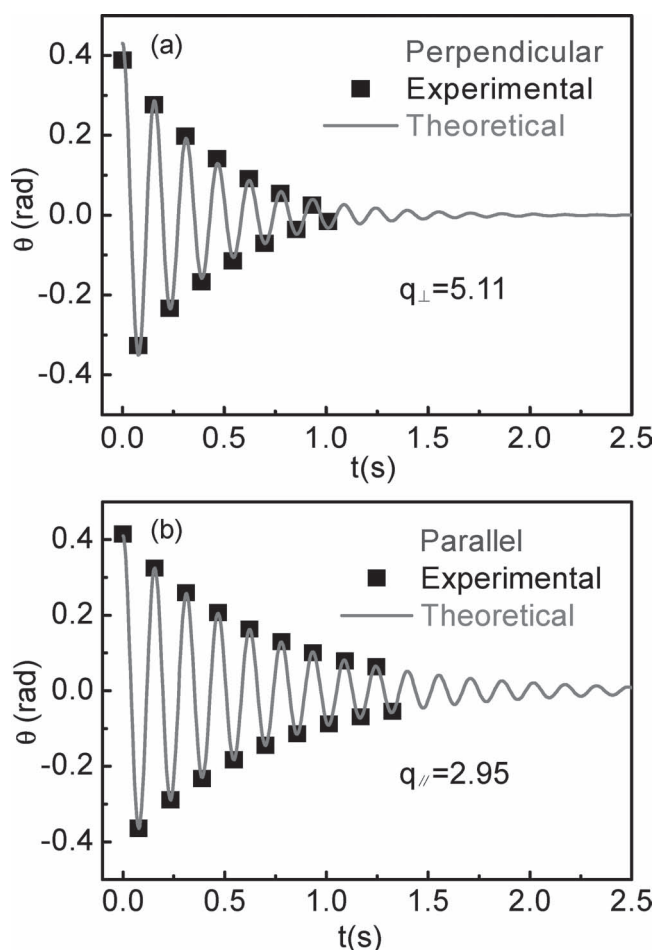


**Figure 5.** Dynamic oscillating curve along the perpendicular and parallel directions. The black squares represent the measured results and the red curve is the theoretical simulation. The damping coefficient in the perpendicular direction is much larger than that in the parallel direction.

## 3. Conclusion

We proposed a three-level structure model of the real rice leaf; macrogrooves, micropapilla, and nanostructures. All the three kinds of structures make their own contribution to the anisotropic sliding behavior of a rice leaf. According to this new model, artificial rice leaves were prepared by combining micro/nanostructures and macrogrooves produced by photolithography, PDMS imprint lithography, and micro/nanostructure coating. To characterize the small sliding angles associated with the weak frictional interaction between the water droplet and the rough surface, we proposed a new method called curvature-assisted droplet oscillation (CADO), which makes it possible to quantitatively characterize the anisotropic dynamic behavior. These results not only provide new insights into the anisotropic sliding phenomenon of the rice leaf, but also are beneficial for the design of controllable biomimetic surfaces for bioinspired system applications.

## 4. Experimental Section

**Fabrication of ARLs:** The epoxy negative resin SU-8 2150 was purchased from Nano MicroChem Company (American). Figure 2a shows the

fabrication scheme of the flexible rice leaf. First, glass substrates were cleaned with acetone, absolute ethanol, and deionized water. A layer (ca. 10  $\mu\text{m}$  or ca. 20  $\mu\text{m}$ ) of SU-8 resin diluted with cyclopentanone (2:1 by weight) was spin-coated onto the slides at 1200 and 600  $\text{rpm min}^{-1}$  and placed in an oven at 95°C for 1 h. The slides were then removed from the oven and cooled to room temperature. To meet the thickness demands of the structure, a second (ca. 20  $\mu\text{m}$ ) and third layer (ca. 20  $\mu\text{m}$ ) were spin-coated onto the solidified samples at 600  $\text{rpm}$  and baked in an oven at 95°C for 1 h to evaporate the solvent. Thus, photoresists of different thickness (10, 20, 40, and 60  $\mu\text{m}$ ) were obtained. Second, groove arrays in 5 $\times$ 5 mm square size with different widths (20, 50, 100, 150, and 200  $\mu\text{m}$ ) were fabricated by photolithography. After exposure, the sample was baked for 10 min and developed in the SU-8 developer for 10 min. Third, the regular groove-array template was sealed with a layer of PDMS precursor liquid mixed with the curing agent (10:1 by weight) and cured at 60°C for 3 h. Here, PDMS Sylgard 184 purchased from Dow Corning (MI) was chosen for its good elasticity, high optical transmission, and biocompatibility. Finally, the peeled-off groove replica was pressed into a pool of nanoporous polydivinylbenzene powder.<sup>[23]</sup> After uncovering, ARLs with macrogroove arrays and composite micro/nanostructures were made. As the nanoporous polydivinylbenzene has strong water resistance, the typical process of low-energy modification was not needed.

**Sample Characterization:** The SA measurements were made by using a Contact Angle System OCA 20 (DataPhysics Instruments GmbH, Germany) at ambient temperature. The SAs were measured by the sessile-drop method with a water droplet (4  $\mu\text{L}$ ). The morphology of the ARL was characterized using a field-emission SEM (JSM-7500F, JEOL, Japan).

## Supporting Information

Supporting Information is available from the Wiley Online Library or from the author.

## Acknowledgements

The authors gratefully acknowledge support from the NSFC under grant nos. 60525412, 90923037, and 60677016.

Received: December 28, 2010

Revised: March 7, 2011

Published online: May 3, 2011

- [1] X. Gao, L. Jiang, *Nature* **2004**, 432, 36.  
 [2] Y. Zheng, X. Gao, L. Jiang, *Soft Matter* **2007**, 3, 178  
 [3] L. Feng, S. H. Li, Y. S. Li, H. J. Li, L. J. Zhang, J. Zhai, Y. L. Song, B. Q. Liu, L. Jiang, D. B. Zhu, *Adv. Mater.* **2002**, 14, 1857.  
 [4] a) O. Sandre, L. G. Talini, A. Ajdari, J. Prost, P. Silberzan, *Phys. Rev. E* **1999**, 60, 2964; b) A. Shastry, M. J. Case, K. F. Bohringer, *Langmuir* **2006**, 22, 6161; c) J. Zhang, Z. Cheng, Y. Zheng, L. Jiang, *Appl. Phys. Lett.* **2009**, 94, 144104; d) N. A. Malvadar, M. J. Hancock, K. Sekeroglu, W. J. Dressick, M. C. Demirel, *Nat. Mater.* **2010**, 9, 1023; e) X. Yao, Q. Chen, L. Xu, Q. Li, Y. Song, X. Gao, D. Quere, L. Jiang, *Adv. Funct. Mater.* **2010**, 20, 656.  
 [5] a) H. Gau, S. Herminghaus, P. Lenz, R. Lipowsky, *Science* **1999**, 283, 46; b) Q. F. Xu, J. N. Wang, L. H. Smith, K. D. Sanderson, *Appl. Phys. Lett.* **2008**, 93, 233112.  
 [6] a) B. Zhao, J. S. Moore, D. J. Beebe, *Science* **2001**, 291, 1023; b) A. M. Higgins, R. A. L. Jones, *Nature* **2000**, 404, 476; c) R. Seemann, M. Brinkmann, E. J. Kramer, F. F. Lange, R. Lipowsky, *Proc. Natl. Acad. Sci. U.S.A.* **2005**, 102, 1848.

- [7] M. Morita, T. Koga, H. Otsuka, A. Takahara, *Langmuir* **2005**, 21, 911.  
 [8] A. D. Sommers, A. M. Jacobi, *J. Micromech. Microeng.* **2006**, 16, 1571.  
 [9] J. Y. Chung, J. P. Youngblood, C. M. Stafford, *Soft Matter* **2007**, 3, 1163.  
 [10] H. Wu, R. Zhang, Y. Sun, D. D. Lin, Z. Q. Sun, W. Pan, P. Downs, *Soft Matter* **2008**, 4, 2429.  
 [11] a) Y. Zhao, Q. H. Lu, M. Li, X. Li, *Langmuir* **2007**, 23, 6212; b) D. Wu, Q. Chen, D. J. Yao, Y. C. Guan, J. N. Wang, L. G. Niu, H. H. Fang, H. B. Sun, *Appl. Phys. Lett.* **2010**, 96, 053704; c) S. Z. Wu, D. Wu, J. Yao, Q. D. Chen, J. N. Wang, L. G. Niu, H. H. Fang, H. B. Sun, *Langmuir* **2010**, 26, 12012; d) S. Z. Wu, J. N. Wang, L. G. Niu, J. Yao, D. Wu, A. W. Li, *Appl. Phys. Lett.* **2011**, 98, 081902.  
 [12] a) D. Y. Xia, S. R. J. Brueck, *Nano Lett.* **2008**, 8, 2819; b) D. Y. Xia, X. He, Y. B. Jiang, G. P. Lopez, S. R. J. Brueck, *Langmuir* **2010**, 26, 2700.  
 [13] a) F. Chen, D. S. Zhang, Q. Yang, X. Wang, B. Dai, X. Li, X. Hao, Y. Ding, J. Si, X. Hou, *Langmuir* **2010**, 27, 359; b) T. Wang, X. Li, J. Zhang, X. Wang, X. Zhang, X. Zhang, D. Zhu, Y. Hao, Z. Ren, B. Yang, *Langmuir* **2010**, 26, 13715; c) F. Zhang, H. Y. Low, *Langmuir* **2007**, 23, 7793; d) J. Yang, F. R. A. J. Rose, N. Gadegaard, M. R. Alexander, *Langmuir* **2009**, 25, 2567; e) Z. Yoshimitsu, A. Nakajima, T. Watanabe, K. Hashimoto, *Langmuir* **2002**, 18, 5818.  
 [14] a) A. Lafuma, D. Quéré, *Nat. Mater.* **2003**, 2, 457; b) W. L. Min, B. Jiang, P. Jiang, *Adv. Mater.* **2008**, 20, 3914; c) A. Winkleman, G. Gotesman, A. Yoffe, R. Naaman, *Nano Lett.* **2008**, 8, 1241; d) S. J. Choi, K. Y. Suh, H. H. Lee, *J. Am. Chem. Soc.* **2008**, 130, 6312.  
 [15] a) M. Nosonovsky, B. Bhushan, *Adv. Funct. Mater.* **2008**, 18, 843. b) D. Wu, Q. D. Chen, H. Xia, J. Jiao, B. B. Xu, X. F. Lin, Y. Xu, H. B. Sun, *Soft Matter* **2010**, 6, 263; c) Y. Lai, X. Gao, H. Zhuang, J. Huang, C. Lin, L. Jiang, *Adv. Mater.* **2009**, 21, 3799.  
 [16] a) J. Hong, W. K. Bae, H. Lee, S. Oh, K. Char, F. Caruso, J. Cho, *Adv. Mater.* **2007**, 19, 4364; b) V. Zorba, E. Stratakis, M. Barberoglou, E. Spanakis, P. Tzanetakis, S. H. Anastasiadis, C. Fotakis, *Adv. Mater.* **2008**, 20, 4049.  
 [17] a) L. Zhai, F. C. Cebeci, R. E. Cohen, M. F. Rubner, *Nano Lett.* **2004**, 4, 1349; b) L. Gao, T. J. McCarthy, *J. Am. Chem. Soc.* **2006**, 128, 9052; c) J. Bravo, L. Zhai, Z. Wu, R. E. Cohen, M. F. Rubner, *Langmuir* **2007**, 23, 7298.  
 [18] L. J. Ci, S. M. Manikoth, X. S. Li, R. Vajtai, P. M. Ajayan, *Adv. Mater.* **2007**, 19, 3300  
 [19] a) Z. Z. Luo, Z. Z. Zhang, L. T. Hu, W. M. Liu, Z. G. Guo, H. J. Zhang, W. J. Wang, *Adv. Mater.* **2008**, 20, 970; b) H. S. Lim, S. G. Lee, D. H. Lee, D. Y. Lee, S. Lee, K. Cho, *Adv. Mater.* **2008**, 20, 4438; c) W. K. Cho, I. S. Choi, *Adv. Funct. Mater.* **2008**, 18, 1089.  
 [20] a) V. Jokinen, L. Sainiemi, S. Franssila, *Adv. Mater.* **2008**, 20, 3453; b) Y. Lee, S. H. Park, J. K. Lee, *Adv. Mater.* **2007**, 19, 2330; c) I. A. Larmour, S. E. J. Bell, G. C. Saunders, *Angew. Chem. Int. Ed.* **2007**, 46, 1710.  
 [21] a) X. Yu, Z. Q. Wang, Y. G. Jiang, F. Shi, X. Zhang, *Adv. Mater.* **2005**, 17, 1289; b) D. Wu, S. Z. Wu, Q. D. Chen, Y. L. Zhang, J. Yao, X. Yao, L. G. Niu, J. N. Wang, L. Jiang, H. B. Sun, *Adv. Mater.* **2010**, 23, 545.  
 [22] a) G. Fraenkel, F. Fallil, K. S. Kumarasinghe, *Entomol. Exp. Appl.* **1981**, 29, 147; b) J. Gao, Y. Liu, H. Xu, Z. Wang, X. Zhang, *Langmuir* **2010**, 26, 9673.  
 [23] Y. L. Zhang, S. Wei, F. J. Liu, Y. C. Du, S. Liu, Y. Y. Ji, T. Yokoi, T. Tatsumi, F. S. Xiao, *Nano Today* **2009**, 4, 135.  
 [24] S. S. Liu, S. D. Liu, *Non-Linear Equations in Physics*, Peking University Press, Beijing, China **2000**.